Materials Horizons

ROYAL SOCIETY OF CHEMISTRY

COMMUNICATION

View Article Online
View Journal | View Issue

Cite this: *Mater. Horiz.*, 2023, 10, 3610

Received 23rd April 2023,
Accepted 9th June 2023

DOI: 10.1039/d3mh00612c

rsc.li/materials-horizons

A liquid-free conducting ionoelastomer for 3D printable multifunctional self-healing electronic skin with tactile sensing capabilities†

Qirui Wu,[ab] Yidan Xu,[c] Songjiu Han,[ab] Jundong Zhu,[a] Anbang Chen,[a] Jiayu Zhang,[a] Yujia Chen,[a] Xiaoxiang Yang,[b] Jianren Huang *[ab] and Lunhui Guan *[ad]

Conductive elastomers with both softness and conductivity are widely used in the field of flexible electronics. Nonetheless, conductive elastomers typically exhibit prominent problems such as solvent volatilization and leakage, and poor mechanical and conductive properties, which limit their applications in electronic skin (e-skin). In this work, a liquid-free conductive ionogel (LFCIg) with excellent performance was fabricated by utilizing the innovative double network design approach based on a deep eutectic solvent (DES). The double-network LFCIg is cross-linked by dynamic non-covalent bonds, which exhibit excellent mechanical properties (2100% strain while sustaining a fracture strength of 1.23 MPa) and >90% self-healing efficiency, and a superb electrical conductivity of 23.3 mS m^{-1} and 3D printability. Moreover, the conductive elastomer based on LFCIg has been developed into a stretchable strain sensor that achieves accurate response recognition, classification, and identification of different robot gestures. More impressively, an e-skin with tactile sensing functions is produced by *in situ* 3D printing of sensor arrays on flexible electrodes to detect light weight objects and recognize the resulting spatial pressure variations. Collectively, the results demonstrate that the designed LFCIg has unparalleled advantages and presents wide application potential in flexible robotics, e-skin and physiological signal monitoring.

New concepts

Electronic skin (e-skin) with tactile sensing function has always been a hot topic in the research on flexible electronic devices. Currently, flexible electronic devices are steadily progressing in a more personalized, functional, and comfortable direction. Traditional flexible e-skin is typically fabricated using lithography, deposition, and erosion techniques, which require a number of demanding technological requirements. DLP-3D printing has been successfully applied to sensors and electronic skins because of its ability to create all in one complex structures without the need for cumbersome processes to achieve patterned design of different functions. However, the development of ionogels based on DLP-3D printing technology is still an urgent contradiction to be solved. Herein, we designed a liquid-free ionogel that can be DLP-3D printed, which is one of the most comprehensive liquid free ionic gels reported to date. Using this material, our 3D-printed flexible e-skin demonstrates its ability to detect lightweight objects and identify the resulting changes in spatial pressure. Collectively, the excellent properties of the material and the flexible application of additive manufacturing processes provide a broad prospect for the development of wearable and intelligent flexible electronic devices.

1. Introduction

Conductive elastomers presented obvious advantages in the field of multi-functional flexible electronic devices, such as artificial skin, electroluminescent devices, wearables and micro-nanogenerators.[1–10] As a new conductive material, elastomers can detect external stimuli caused by stretching, bending and twisting, and convert them into corresponding electrical signals such as resistance, capacitance, and current.[11–15] Currently, most reported conductive elastomers are mainly divided into two kinds: hydrogel-based and ionogel-based. The former is favored for its excellent mechanical and electrical performance, but it loses the function of electronic devices because the solvent evaporates easily.[16–22] The latter, consisting mainly of ionic liquids (ILs), are at risk of liquid leakage despite exhibiting negligible vapor pressure and non-volatile properties.[23,24] In addition, conductive additives (*e.g.*, conductive polymers, carbon-based materials, and metal materials) are often added to an elastomer matrix in order to endow flexible materials with superb electrical conductivity. However, the introduction of conductive fillers is accompanied by tradeoffs between mechanical and electrical properties, as the two properties are often contradictory

[a] CAS Key Laboratory of Design and Assembly of Functional Nanostructures, Fujian Key Laboratory of Nanomaterials, Fujian Institute of Research on the Structure of Matter, Chinese Academy of Sciences, Fuzhou 350108, China
[b] School of Mechanical Engineering and Automation, Fuzhou University, Fuzhou 350108, China
[c] Department of Oncology, The First Affiliated Hospital of Anhui Medical University, Hefei 230000, China
[d] A College of Chemistry, Fuzhou University, Fuzhou 350108, China

† Electronic supplementary information (ESI) available. See DOI: https://doi.org/10.1039/d3mh00612c

in a material system. Consequently, it remains a great challenge to prepare a multifunctional flexible sensor with admirable stability, mechanical properties and electrical properties.

A deep eutectic solvent (DES) is a new green, non-toxic and harmless solution formed by hydrogen bond acceptors and donors.[25–28] As the investigation progressed, it came to light that the potential applications of DES could be expanded through *in situ* photopolymerization to create a polymerizable deep eutectic solvent (PDES).[24,29] This discovery had made PDES a promising candidate for flexible conductive elastomers. Wang *et al.* prepared CNF/PDES conductive elastomers using a one-pot method, in which the introduction of CNF improved the elastic modulus and toughness of composite elastomers, so as to be better applied to wearable devices.[30] Sun *et al.* fabricated a series of ionoelastomers with excellent electrical and mechanical properties based on DES and applied them to human motion detection.[31] While the PDES elastomer exhibits outstanding performance, there is still a need to enhance its mechanical and electrical characteristics and stability in order to meet the requirements of various applications.

Currently, flexible electronic devices are steadily progressing in a more personalized, functional, and comfortable direction.[32] Traditional flexible wearables are typically fabricated using lithography, deposition, and erosion techniques, which requires a number of demanding technological requirements.[5,33–35] Thanks to its ability to create complex structures, 3D printing is used successfully in flexible robots, sensors and electronic skins (e-skins).[36–40] Digital light processing (DLP) stands out among the different 3D printing technologies due to its significant advantages, which encompass rapid printing speed, superior resolution, and affordable cost.[14,21,24,41] Moreover, personalized manufacturing of flexible functional devices through 3D printing technology has attracted much attention, but the development of ionogels based on DLP-3D printing technology is still an urgent contradiction to be solved.

Herein, we fabricated a liquid-free conductive ionogel (LFCIg) with excellent performance, utilizing the innovative double network design approach based on a deep eutectic solvent (DES). In the LFCIg system, gelatin as a rigid network and together with a supramolecular DES polymer network forms a double network skeleton. And there were multiple dynamic non covalent crosslinks between different components, obtaining conductive elastomers with excellent performance, including outstanding mechanical strength (2100% strain while sustaining 1.23 MPa fracture strength), superb electrical conductivity (23.3 mS m^{-1}) and wonderful 3D printability. Simultaneously, LFCIg exhibiting other properties such as non-volatility, self-healing, and so on were regarded as the icing on the cake to endow the additional stability for flexible electronic device. This is one of the best liquid-free ionogels with comprehensive properties reported so far. Additionally, a flexible tensile strain sensor based on LFCIg has been developed to recognize the gestures from robots, which can quickly convert mechanical stimuli into electrical signals to demonstrate potential applications in flexible wearable devices. Interestingly, an e-skin with tactile sensing functions was produced by *in situ* 3D printing of sensor arrays on flexible electrodes reproduced by screen printing. The entire process only required additive manufacturing without any other cumbersome processes. The tactile sensing system for e-skins demonstrates its ability to detect light weight objects and recognizes the resulting spatial pressure variations. Collectively, the excellent properties of the material and the flexible application of the additive manufacturing process provide a broad prospect for the development of wearable and intelligent flexible electronic devices.

2. Results and discussion

2.1 Synthesis and characterization of LFCIgs

The double-network LFCIg with great strength, ionic conductivity, stretchability, self-healing and were successfully fabricated by polymerizing PDES monomers composed of acrylic acid (AA) and choline chloride (ChCl) in the presence of gelatin, and poly (ethylene glycol) diacrylate (PEGDA). First, AA and ChCl were polymerized to form a supramolecular deep eutectic polymer network where the solid ChCl acts as a hydrogen bond acceptor and forms a tight hydrogen bond link with the hydrogen bond donor AA. Notably, the PEGDA was introduced into the gel system as a cross-linker to covalently connect ionic monomers for making them exhibit soft texture and excellent stretchability. Furthermore, gelatin networks, which can be dissolved in transparent PDES liquid at 90 °C, were treated as a rigid network and together with supramolecular deep eutectic polymer network to form the double network skeleton of LFCIg (Fig. 1(a)). In detail, the gelatin molecular chain contains a large number of amino acid residues, providing abundant hydrogen bonding sites, so that the non-covalent interaction between different molecular chains was enhanced. Crucially, there was no volatile liquid filling the ionogel network during this process. Thereafter, the LFCIg precursor solution was then mixed with photoinitiator 819 to rapidly fabricate LFCIg in 20 s *via in situ* photopolymerization. Unfortunately, thanks to the violent polymerization reaction of the precursor solution, a large amount of thermal energy was released, which was detrimental to the preparation of LFCIg and subsequent work. Fig. S1 (ESI†) clarified the inks with and without tartrazine before photo-curing. Accordingly, tartrazine was selected as the pigment to absorb, reflect and scatter UV light, which made the photopolymerization time and the highest temperature severely extended to 40 s and 47.7 °C due to reduction in the efficiency of the photoinitiator (Fig. S2, ESI†). In the ionogel systems, there are a large number of hydrogen bonding sites between the double networks, so that the formation of multiple hydrogen bonds (Fig. 1(b)) between the functional groups (*e.g.*, carboxyl, amino, hydroxyl, chloridion, *etc.*), which not only intensifies the non-covalent interaction, but also enhances the self-healing. In addition, LFCIg exhibited excellent elasticity, with the ability to accommodate any bending, twisting and stretching movements (Fig. 1(c)).

To confirm the interaction and structural evolution of the networks within the ionogel systems, a Fourier transform

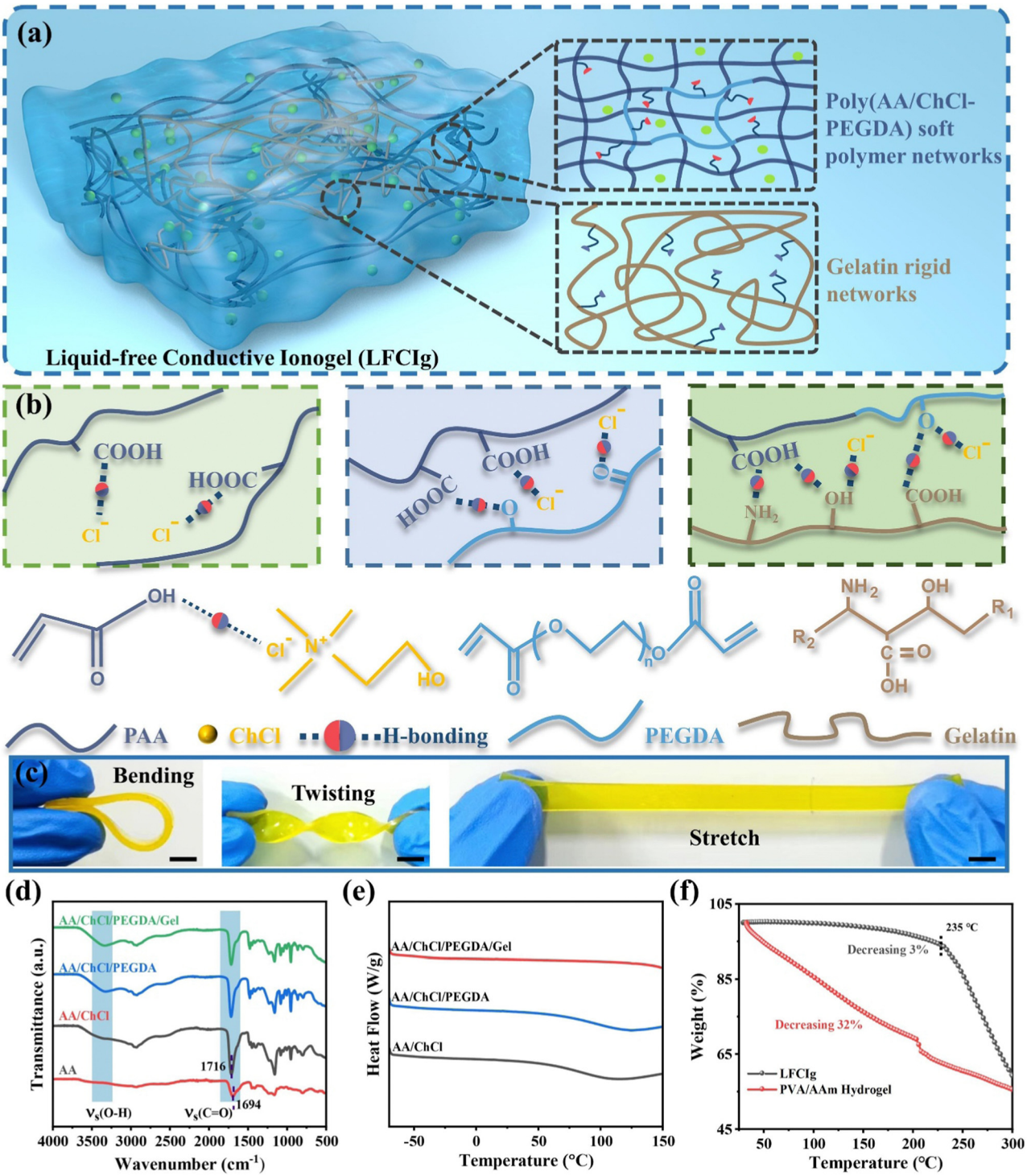

Fig. 1 Synthesis principle and physical properties of the double-network LFCIg. (a) Schematic illustration of composition of in LFCIg. (b) Schematic of the multiple hydrogen bond interactions between the various components in the LFCIg. (c) Mechanical behaviour of LFCIg, including bending, twisting, and stretching. Characterization of the LFICIg with different components: (d) FT-IR spectra; (e) DSC; (f) TGA. The scale bar is 5 mm.

infrared (FT-IR) platform was utilized to test the photocured specimens of various components. Fig. 1(d) clearly demonstrates that as each component was gradually added, a significant and broad peak emerged within the range of 2500 to 3500 cm^{-1}. Moreover, the non-covalent interaction between the different components led to an increase in the peak value of the characteristic absorption peak at 3300 cm^{-1}, which is attributed to the stretching vibrations of the hydroxyl group.[41] Simultaneously, a shift in the vibration peak caused by C=O from 1694 cm^{-1} in polyacrylic acid to 1716 cm^{-1} in LFCIg was

observed, which is attributed to the strong electronegativity of chloridion and the induction effect.[27] To summarize, the above results illuminate the existence of abundant hydrogen bonding in LFCIg, which reinforced the interrelation among the various functional groups and enables wonderful mechanical properties to be exhibited.

In order to reveal the change of phase transition behavior of LFCIg after the introduction of different components, the differential scanning calorimetry (DSC) data were collected for both pure PDES and LFCIg with gradual addition of PEGDA and gelatin. As manifested in Fig. 1(e), the DSC curve profiles showed that non-crystallization peak appeared in the temperature range of −70 to 150 °C, revealing the amorphous structure. Strikingly, the DSC showed that LFCIg did not undergo phase transition at low temperature, which indicated that the ionic gel maintained good elastic properties. Similarly, the XRD results demonstrated broad diffraction peaks at $2\theta = 20^\circ$ (Fig. S3, ESI†), which further confirms the non-crystalline characteristic of LFCIg.[42] Furthermore, the thermal gravimetric analysis (TGA) results show that the initial decomposition temperature of LFCIg was ∼235 °C, indicating that the material has superior thermal stability. In comparison to the classic PVA/AAm hydrogels, which exhibited a significant weight loss of 32% before reaching a temperature of 200 °C, LFCIg demonstrated a negligible reduction of only 3%. The LFCIg appeared excellent performance at extreme temperatures, which boils down to the absence of exudation of volatile liquid in LFCIg and the stable double network structure formed by PDES after participating in polymerization. The LFCIg and PVA/AAm hydrogels were stored at 80 °C, while the material weight changes were recorded continuously for 75 hours. As manifested in Fig. S4 (ESI†), the mass of LFCIg after storage showed negligible changes and maintained the same elasticity as the original specimen. In contrast, PVA/AAm hydrogels gradually stiffened on account of severe mass loss.

2.2 Electrical, mechanical, and self-healing properties

By adjusting the molar ratio of copolymer AA to ChCl (1 : 0.2, 0.4, 0.6), a series of LFCIg with different properties were obtained. Firstly, mechanical properties are one of the most critical factors in the field of flexible sensors. Therefore, the mechanical properties of the ionogel materials prepared were evaluated *via* the uniaxial tensile test at room temperature. As is evident in Fig. 2(a) and (b), the tensile strength of the LFCIg obtained decreased from 4.73 ± 0.05 to 1.23 ± 0.01 MPa as the ChCl molar increased, while the fracture strain increased from 1305 ± 45 to 2100 ± 50%. In addition, the Young's modulus of the ionogels showed a similar pattern of changes, decreasing from 2.35 ± 0.06 to 0.27 ± 0.05 MPa as the molar ratio of ChCl increased (detailed information is provided in Fig. S5 and Table S3, ESI†). This phenomenon is attributed to the increased density of hydrogen bonds in the LFCIg. In detail, with the increasing of ChCl content, the hydrogen bond density inside LFCIg gradually heightens, which leads to the possibility of hydrogen bond rearrangement during the deformation of the elastomer, thus enhancing the ductility of the ionogel and the flexibility of the composite material. The results obtained are consistent with those previously reported.[30,43] In general, the flexible materials used in soft robots typically require a Young's modulus within the range of 0.1–10 MPa, along with an ultimate tensile strain of >200%. Therefore, the synthesized LFCIg fully met or even exceeded the expectation. As demonstrated in Fig. S6a (ESI†), sandwiched between two pieces of the electrode were ionogels whose conductivity was measured using electrochemical impedance spectroscopy (EIS). As depicted in the Nyquist diagram (Fig. S6b, ESI†), an increase in ChCl content resulted in a corresponding enhance in ionogel conductivity, which rose from 5.7 to 23.3 mS m^{-1}. It is noteworthy that the electrical conductivity and stretchability of the designed LFCIg were significantly enhanced with an increase in ChCl content, which was uncommon in ionogel systems where these properties were typically mutually exclusive. Specifically, in order to achieve extremely high conductivity in ionogels, a large quantity of conductive additives is often added during material synthesis, which can cause the transition of the ionogel from an elastic to a plastic state. Furthermore, the addition of ChCl to the ionogel as a soft chain segment enhanced the flexibility of the polymer network and thus improved the conductivity, which boils down to the soft chain segment providing more space beneficial to the movement of conductive ions.[44] Compared with the most advanced liquid-free ionic conducting elastomers, our synthetic LFCIg films showed outstanding electrical conductivity while providing excellent tensile and fracture strength under ambient conditions (Fig. 2(c)). While previous studies had confirmed either high electrical conductivity or good tensile properties in ionogels, it was rare to find a combination of all three properties in a single material. To summarize, we successfully synthesized ionogels without the presence of any liquid phase and achieved superb mechanical and electrical properties. The ionogels containing 0.6 mol of ChCl provided remarkable fracture strength of 1.23 MPa, while maintaining a stretchability of 2100% strain and electrical conductivity of 23.3 mS m^{-1} (Table S3, ESI†). Hence, this optimized formula was used in subsequent experiments.

In addition to mechanical properties, self-recovery is an important characteristic affecting the durability of an elastomer. We tested the self-recovery properties of LFCIg through a series of tensile cycle tests. As shown in Fig. S7a (ESI†), LFCIg demonstrated the ability to easily recover from strains ranging from small (200%) to large (800%) strains, which boiled down to its self-recovery properties which were endowed by cross-linking through reversible non-covalent bonds. The hysteresis loop below the stress–strain curve show the energy dissipated when multiple hydrogen bonds break during the stretching process. It is noteworthy that the hysteresis loop area was positively correlated with the strain, which meant that more energy is consumed under large strain to avoid the damage of ionogel. The tensile strength of LFCIg improved from 200 to 800% strain, the dissipated energy increased sharply from 0.17 to 1.62 MJ m^{-3}, and the energy dissipation coefficient stabilizes from 55% to the final 37% (Fig. S7b, ESI†). Moreover, the energy dissipation coefficient of large strain was lower than that of the small strain, which was mainly put down to the

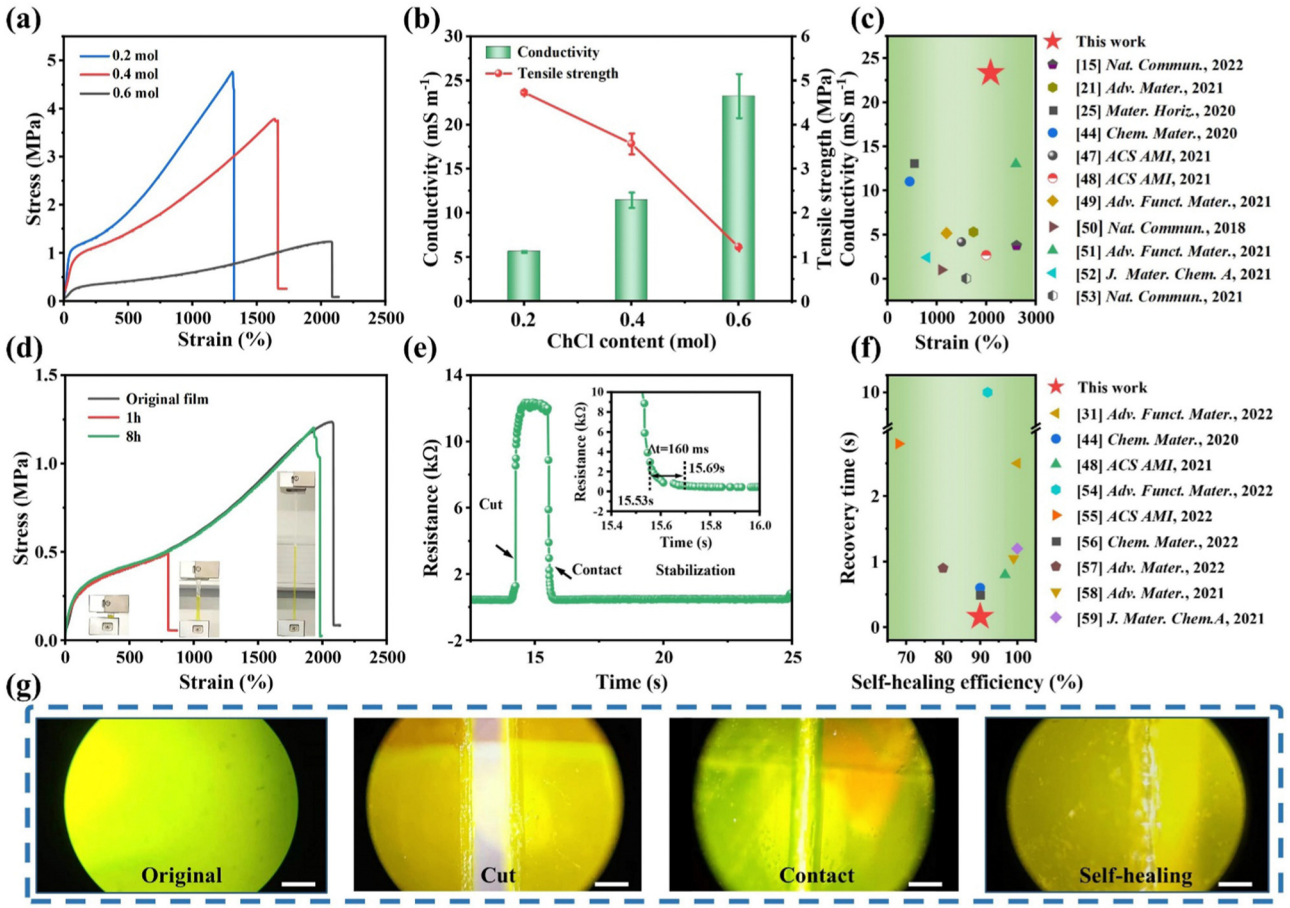

Fig. 2 (a) The stress–strain curves of LFCIg with different ChCl contents. (b) Conductivity and tensile strength of ionogels with different ChCl contents. (c) Comparison of the LFCIg with previously studied materials in terms of conductivity and strain.[15,21,25,44,47–53] The details are presented in Table S1 of the ESI.† (d) Stress–stretch curves of the original film and healed specimens. (e) Resistance changes of LFCIg during the cutting and contacting process. (f) Comparison of the LFCIg with previously studied materials in terms of recovery time and self-healing efficiency.[31,44,48,54–59] The details are presented in Table S2 of the ESI.† (g) Self-healing process of ionogel. The scale bar is 500 μm.

synergistic strategy between dynamic hydrogen bonds through reversible deformation leading to energy dissipation and covalent bonds maintaining structural stability. To summarize, there were a large number of multiple reversible bonds (ionic interactions, and hydrogen bonding) between AA, ChCl and gelatin in ionogels, which acted as sacrificial bonds and inclined to be wrecked preferentially to dissipate energy efficiently when small strain was applied.[45] Thereafter, the covalent bond was irreversibly broken due to the increase of dissipated energy at the applied large strain (Fig. S8, ESI†). Moreover, the self-recovery performance was evaluated by performing cyclic loading experiments with 200% strain on the ionogel for a given interval of rest between consecutive cycles. As featured in Fig. S7c and d (ESI†), the cyclic curve of the ionogel gradually approached the initial curve after resting time, which boils down to the reconstruction of dynamic hydrogen bonding over time. After standing for 10 min, the maximum stress of the ionogel recovered to 0.21 MPa, close to the first loading value of 0.23 MPa, indicating the fine self-recovery ability of the ionogel. In addition, the LFCIg was tested 10 times consecutive loading–unloading cycles, and the cyclic curve elucidated obvious hysteretic and 75% residual strain (Fig. S7e and f, ESI†). During the first cycle, a larger hysteresis loop was observed, whereas the hysteresis region decreases significantly during the next 2–10 cycles. This phenomenon could be explained by the fact that some of the dissociated dynamic bonds from the first cycle had not completely recovered. Self-healing is another highly desirable material property of LFCIg because it helps extend the lifetime of materials and equipment, especially in complex environments. Strips of ionogel were dyed with tartrazine and cut in half, then brought back into contact at 60 °C. It is important to note that the introduction of tartrazine does not affect the mechanical properties of the material (Fig. S9, ESI†). Intriguingly, the self-healing process of LFCIg was observed under an optical microscope, and it was obvious that the ionogels displayed superb self-healing ability without any external stimulation (Fig. 2(f)). Additionally, the tensile tests were performed on LFCIg repaired for 1 and 8 hours to quantitatively assess the self-healing efficiency of ionogel. As depicted in Fig. 2(d), the LFCIg exhibited remarkable mechanical properties even after undergoing an 8 hour healing process. Surprisingly, the breaking strength increased to 1.2 MPa, and the

tensile strain was restored to nearly the same level as the original film, reaching up to 1980%. To the best of our knowledge, this was one of the ionogels that had been documented to exhibit high breaking strength and withstand significant deformations following self-healing. Simultaneously, the self-healing efficiency of LFCIg was defined by the ratio of toughness before and after healing. Upon analysis, it was determined that the sample exhibited a self-healing efficiency of 27% and 90% after 1 h and 8 h, respectively. The self-healing properties of the LFCIg was predominantly determined by dynamic ionic bonds and numerous hydrogen bond interactions between the polymer chains. In detail, the polyphase polymer chain at high temperature was more prone to dynamic ion exchange reaction, and multiple hydrogen bonds in the polyphase polymer chain interact more easily to recombine.[15] Fig. S10 (ESI†) clarified that the ionogel was used in 8 successive cutting–healing processes at the same position to demonstrate its potential applications in the field of electronic devices. Upon cutting the specimen, the resistance value of the ionogel experienced an abrupt increase to an infinite value. However, the resistance value was quickly restored to its original state and remained stable after the fracture contact. Satisfactorily, the whole process could be completed in only 160 ms. This suggests that the ionogel exhibits exceptional self-repairing ability and electrical stability. Certainly, the liquid-free ionogel revealed remarkable performance when compared to current advanced ionogel materials that possess both recovery and self-healing properties (Fig. 2(g)).

2.3 Strain sensing performance and applications of LFCIg

Flexible electronic devices including artificial skin, actuators, sensors, *etc.*, required stable electrical properties, mechanical durability, and self-healing characteristics for potential applications. Fortunately, by utilizing the non-volatile properties of LFCIg, it has been proven that it possesses the ability to serve as a strain sensor with long-term stable monitoring capabilities for human motion. Fig. 3(a) illustrated the correlation between strain and the relative resistance change ($\Delta R/R_0$). The sensitivity of the sensor was evaluated by defining the gauge factor (GF), which was obtained by calculating the slope of the curve showing the shift of $\Delta R/R_0$ *versus* strain, corresponding to the GF of 0.69 (R^2 = 0.995) at 0–200% strain, and was conspicuously heightened to 2.75 (R^2 = 0.997) for the 200–600% strain, respectively. Impressively, the sensor showed terrific sensitivity when the applied strain increased to 1000%, and the corresponding GF (3.54) exhibited a linear relationship with the tensile strain. Furthermore, the performance of the sensor is characterized by its response and recovery time, which are critical factors. Thus, by exploring the immediate response time to the external loading and unloading pressures of the sensor, the LFCIg appeared sensitive response and recovery times of 120 ms and 140 ms, demonstrating its unexceptionable electromechanical performance (Fig. 3(b)). More importantly, compared with other reported conductive ionoelastomer strain sensors, the performance of the sensor developed by us based on LFCIg is significantly superior (Fig. 3(c)). As shown in Fig. S11 (ESI†), the resistance of the ionogel sensor exhibited significant and stable changes during dynamic tensile testing, regardless of whether the test was conducted at low (1–8% strain) or high (50–200% strain) strains, suggesting a high sensitivity across a wide range of strains. Additionally, the sensitivity of LFCIg to velocity was revealed by applying tensile strain (100% strain) at different rates to the sensor. As present in Fig. S12 (ESI†), the LFCIg sensor exhibited a nearly constant $\Delta R/R_0$ even with an increase in the tensile rate from 25 to 200 mm min^{-1}. The results showed that the effect of tensile rate on $\Delta R/R_0$ was negligible, which further proved the universal applicability of the sensor. Besides, the pursuit of reliability and durability in sensors has been ongoing, aiming to guarantee extended periods of employment without any degradation of performance. Thereafter, we performed 1000 stretch–relaxation cycles on the LFCIg sensor, and then confirmed that the electromechanical signal output from the sensor maintained good signal stability throughout the process by enlarging the image of Fig. 3(d) at different time points. By assembling the prepared ionogel into an epidermal strain sensor, the application of LFCIg in human physiological signal monitoring can be further demonstrated. Intriguingly, the sensor was attached to the joint of the robotic finger as shown in Fig. 3(e) to monitor the motion state of the fingers. The manipulator demonstrated ten gesture forms (initial state, ''A'', ''B'', ''C'', ''D'', ''I'', ''L'', ''O'', ''V'', ''E'', and ''Y'') selected from American Sign Language, and the corresponding output response of each gesture form is shown in Fig. 3(f). The robotic finger joint movement was the source of each current signal. These signals exhibited five distinct waveform characteristics for each gesture, which enabled accurate response recognition, classification, and identification. Undoubtedly, the novel concept demonstrated the potential application value of LFCIg in flexible intelligent devices and many other sensing fields.

2.4 3D printing of structured ionogels for application in flexible devices

The one-step photopolymerization of ionogels was utilized to demonstrate its application as a new type of 3D printing ink in flexible electronics. A high precision 3D printing method (Digital Light Processing, DLP) was selected to achieve the fabrication of structured devices for ionogels, which depended on the good fluidity of LFCIg ink. Fig. 4(a) illustrates the working principle of DLP utilizing layer-by-layer accumulation and manufacturing, which was important for the subsequent *in situ* polymerization of flexible sensor arrays. At present, flexible electronic devices are developing towards miniaturization integration, and modularization, which challenges the traditional manufacturing methods. As revealed in Fig. 4(b), we successfully printed a conceptual model of the brain–computer interface with LFCIg ink. The microcircuit exhibited a width of 0.18 mm in the enlarged view, indicating that it had great potential value in the area of flexible electronics. Homoplastically, a model of a porous leaf had been reproduced perfectly, further demonstrating the terrific 3D printability of LFCIg ink. What is important is that currently there is an endless stream of hydrogels that can be 3D printed, but it is

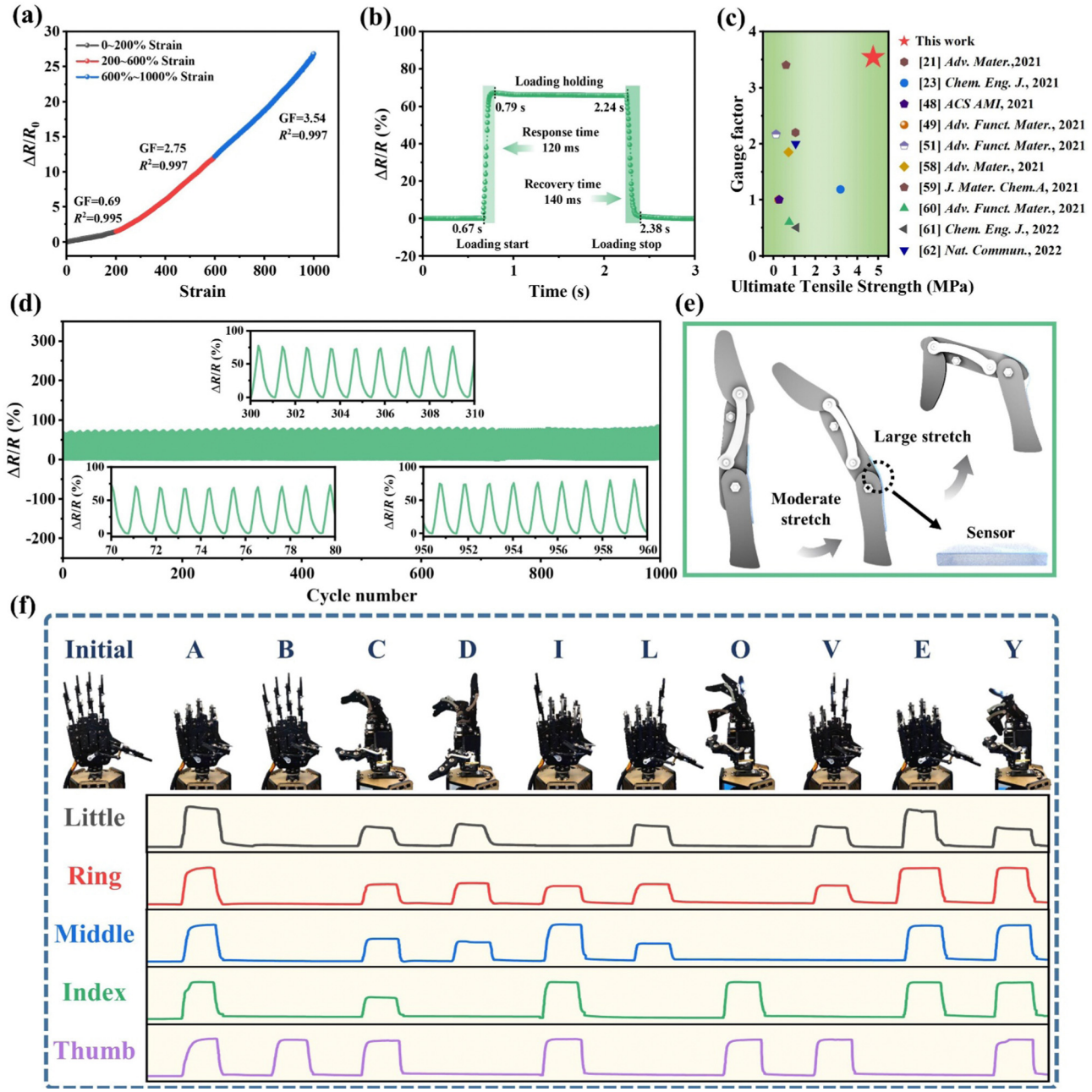

Fig. 3 Electromechanical response of the resistance-type sensor based on LFCIg. (a) Relative resistance change ($\Delta R/R_0$) *versus* strain. (b) The response time required by the LFCIg sensor during loading and unloading. (c) Comparison of the LFCIg with previously studied materials in terms of response time and self-healing efficiency.[21,23,48,49,51,58–62] The details are presented in Table S4 of the ESI.† (d) Relative resistance change ($\Delta R/R_0$) of the LFCIg sensor for 1000 loading–unloading cycles at 100% strain. The LFCIg was attached to the manipulator joint as a sensor to monitor motion signals: (e) diagram of the sensor attached to the joint of the manipulator, and (f) Digital photos of the gesture morphologies and generated current profiles as recognition patterns for 10 gesture morphologies collected by LinkZill 01RC.

extremely rare for liquid free conductive ionogel materials to realize additive manufacturing through DLP-3D printing technology. Additionally, the fabrication of the island-bridge microstructure was achieved without the help of any other cumbersome steps by applying a uniform layer of ionogel ink on a transparent platform (Fig. 4(c)). It is worth mentioning that LFCIg devices can be accurately manufactured in extreme time through DLP-3D printing, regardless of the structural complexity of microelectronic devices. Moreover, the microstructure composed of island-bridge patterns was successfully transferred onto a TPU film, and subsequently connected to an LED lamp *via* a wire. As is evident in Fig. 4(d) and Movie S1 (ESI†), as the microcircuit undergoes more deformation, the corresponding LED lamp changes from bright to dark, indicating that the LFCIg microcircuit exhibits excellent conductivity and stretchability.

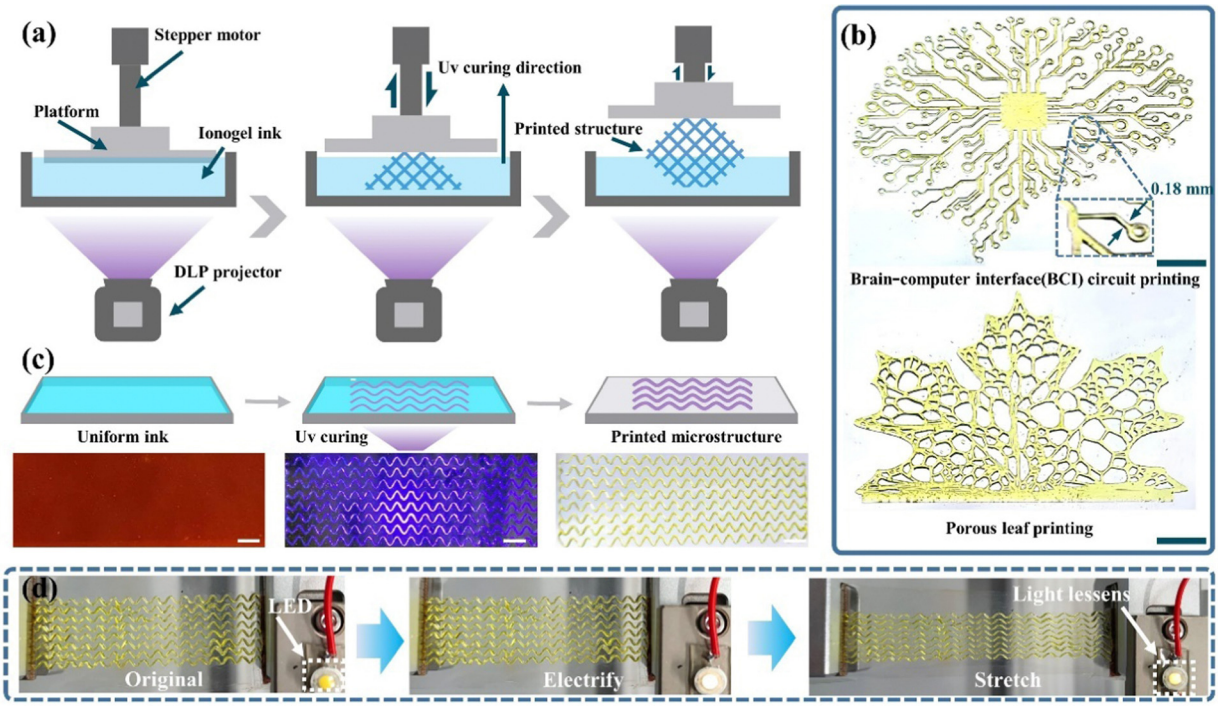

Fig. 4 Fabrication of 3D printing LFCIg based on microstructure design. (a) The process and principle of 3D printing. (b) 3D printing of LFCIg ink-based brain computer interface microcircuit and porous leaf model. (c) The process of 3D printing the island-bridge microcircuit of LFCIg. (d) A visual demonstration of the relationship between good stretchability of island-bridge microcircuit and LED lighting based on LFCIg. All the above scales are 1 cm.

2.5 Tactile sensing system for an e-skin

The single capacitive sensor was assembled by sandwiched between two electrodes with a 1 × 1 cm^2 ionogel (Fig. S13, ESI†). The capacitance meter (TruEbox-01RC, Linkzill) was connected in series to two electrodes *via* a wire and an insulating film was enclosed in the outermost layer of the sensor, endowing sensor with a pressure-perceiving property similar to that of the skin. Based on the results displayed in Fig. 5(a), it can be observed that when the pre-applied pressure was 1.225 kPa, the device demonstrated a clear capacitance variation in response to stepwise application of three distinct pressure levels 490, 245, and 123 Pa. These findings strongly suggest that the capacitive sensor exhibits commendable micro-pressure recognition capability. Observations made during the experiment indicate the presence of slight increments in peak capacitance under applied pressure, which boils down to the persistent aggregation of ions and electrons within the ion–electron capacitive interface.[46] In addition, the assembled sensors are affixed to the throat to unambiguously detect and differentiate the vibrational patterns generated by distinct auditory stimuli (Fig. 5(b)). To assess the dynamic response rate of the newly devised capacitance-type e-skin, a nominal pressure of 1.2 kPa was carefully applied, which was subsequently promptly released to initiate the response and recovery process, culminating in an approximate time span of 100 ms (Fig. 5(c)).

As depicted in Fig. 5(d), to fabricate a tactile sensing system comprising electronic skin with pressure recognition capability, we employed an integrated approach utilizing 3D printing and screen-printing technologies to generate an electronic skin matrix comprised of 8 × 8 pixels. Initially, the conductive carbon paste was deposited onto a flexible PET film in a pattern corresponding to the intended circuit design, using a screen-printed mask as a precise guide. The flexible circuits and electrodes created using conductive carbon paste demonstrated exceptional line impedance, which enabled the series and parallel lighting of LED lights with great efficiency (Movie S2, ESI†). This phenomenon suggested that the flexible circuit and electrode had exceptional conductivity, and any potential impact on signal transmission in the sensor unit could be disregarded. Thereafter, the LFCIg ink was subsequently photopolymerized *in situ* on the carbon electrode *via* DLP-3D printing technology to complete the preparation of the e-skin sensor array (the dimension of pixels is 4 × 4 mm, and the thickness is 500 μm). Then, the flexible circuit, sensor array and Jumper Wire interface were assembled to obtain the electronic skin as shown in Fig. 5(d)-i. The tactile sensing system of the whole electronic skin possessed a structural dimension of 73 mm in length and 46 mm in width (Fig. 5(d)-ii), while retaining its soft and flexible properties (Fig. 5(d)-iii). Furthermore, the e-skin, which was integrated with a layer of PET (100 μm thickness), demonstrated exceptional flexibility, making it a highly adaptable and versatile device for large-scale applications. Fig. 5(e) and Fig. S14a and c (ESI†) displayed optical images of the e-skin with different shapes (C-shaped, A-shaped, and S-shaped) of epoxy blocks placed

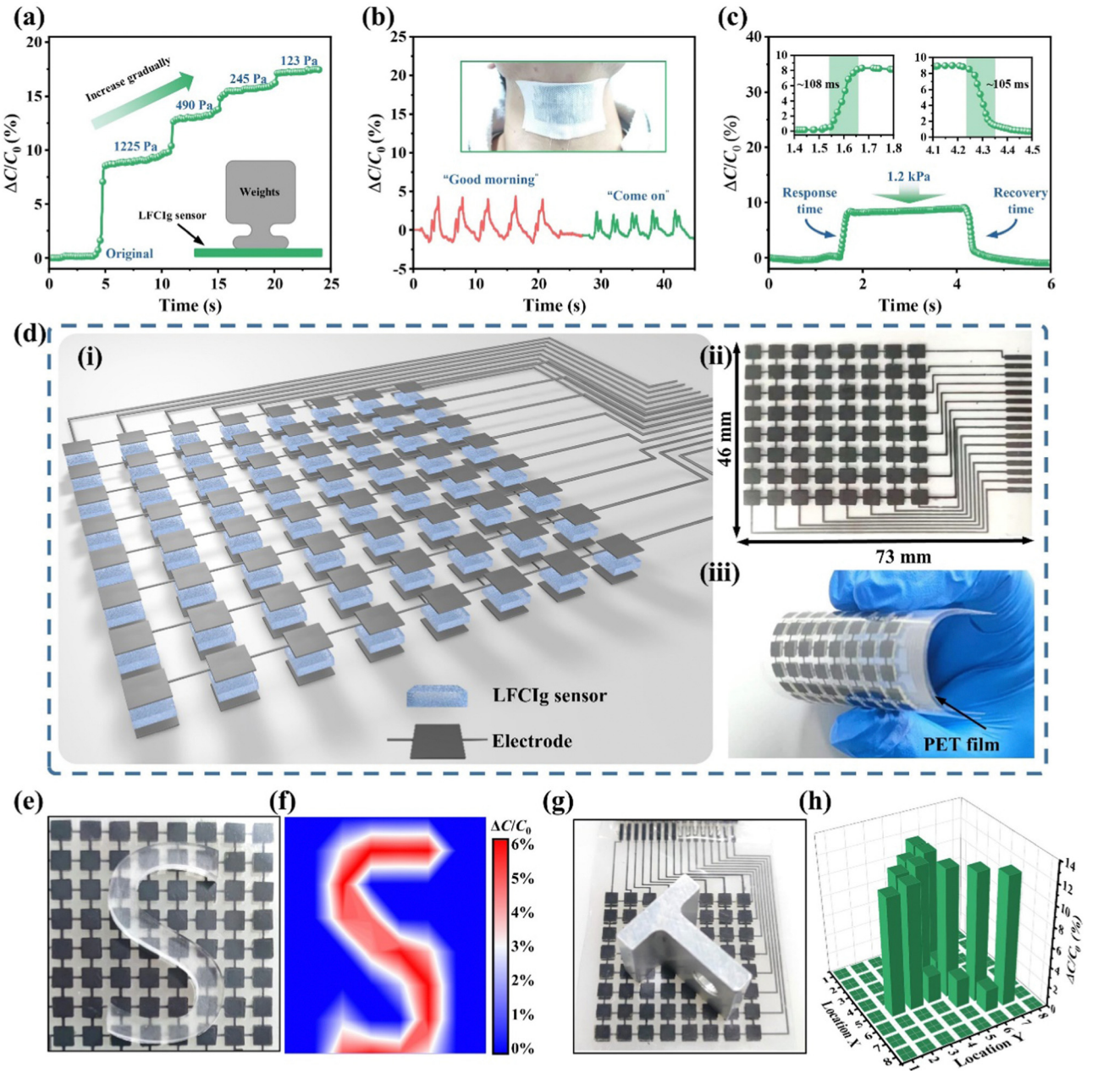

Fig. 5 Tactile sensing system for capacitive electronic skin based on LFCIg. (a) The detection of tiny pressure (123, 245, and 490 Pa) under the load of high pressure (1.225 kPa). (b) Monitor and analyze human speech signals *via* electronic skin. (c) Response and recovery time at a pressure of 1.2 kPa. (d) The establishment of electronic skin tactile sensing system. (e) Optical images of the flexible large-scale e-skin with a S-shaped epoxy resin block on it, and (f) the contour plot of 2D mapping. (g) Optical image showed a flexible electronic skin with a metal block positioned on its surface, and (h) 3D bar charts depict the distribution of pressure that corresponds to the metal block.

on top of it. Correspondingly, the pressure distributions measured by the e-skin are presented in Fig. 5(f) and Fig. S14b and d (ESI†), which demonstrate its ability to detect slight weight objects and recognize the resulting spatial pressure variations. Analogously, Fig. 5(h) depicts T-shaped metal block placed on the e-skin, and the corresponding pressure distribution was presented as a 3D bar chart in order to accurately digitally reconstruct the shape of objects, as shown in Fig. 5(g).

3. Conclusions

In summary, we demonstrate a liquid-free conductive ionogel having a double network of a soft polymer network and a rigid network *via* dynamic non-covalent bonding. This material overcomes several drawbacks associated with traditional ionic conductive materials, as it exhibits remarkable mechanical properties, electrical conductivity, environmental stability, and self-healing capabilities. Furthermore, we demonstrate a flexible stretchable strain sensor based on the highly sensitive

properties of the material, which can accurately collect the gesture motion signals of the robot. These devices are essentially impermeable to leakage and evaporation, ensuring the long-term stable operation of flexible electronic devices. Notably, the LFCIg also demonstrates impressive 3D printing capabilities, allowing for the precise creation of a variety of intricate microstructures. More interestingly, the 3D printing capability of LFCIg was leveraged in combination with screen printing technology to establish an e-skin tactile sensing system with perceptive function. The established e-skin accurately detects and identifies changes in spatial pressure caused by light weight objects, indicating a wide range of potential applications in flexible intelligent devices and numerous other sensing fields.

4. Experimental section

4.1 Materials

Gelatin powder (Gel, bloom ~100), choline chloride (ChCl, 98%) and poly (ethylene glycol) diacrylate (PEGDA, 700) was purchased from Shanghai Macklin Biochemical Co., Ltd; acrylic acid (AAc, 98%) was supplied by Tansoole; the photoinitiator used in this study, phenylbis (2,4,6-trimethylbenzoyl) phosphine oxide (PPO), was purchased from Shanghai Aladdin Biochemical Technology Co., Ltd. All other chemicals, including PDMS, PET film, metal block, conductive carbon paste, and glass plates, were obtained from local suppliers and used as received without any further purification.

4.2 Synthesis of the LFCIg

The precursor solution for the LFCIg was prepared using a one-pot method, in which AAc, ChCl, PEGDA, Gel, and PPO were mixed together. Firstly, AA and ChCl were mixed at different molar ratios at 90 °C for 30min to form a transparent DES solution, then 2 wt% (referred to the mass of DES) Gel and 1 wt% PEGDA were added to DES solution for further heating and stirring for 4 h. When the mixture was cooled to room temperature, 1 wt% PPO and 0.03 wt% tartrazine were introduced respectively and stirred well to form precursor solution. A rubber gasket with a thickness of 1.5 mm was used to separate the glass plates, and the precursor solution was then poured into the mold formed by the glass plates. Finally, the filled glass mold was exposed to ultraviolet light for approximately 8 minutes to produce the ionogel.

4.3 3D printing of LFCIg

The additive manufacturing of LFCIg was realized by purchasing DLP-3D printer (NOVA3D Master) from Shenzhen Nova Intelligent Technology Co., Ltd. The printer shows that the *X*/*Y* printing precision of 50 μm and *Z* precision of 10 μm can meet the requirements of 3D printing of LFCIg. The whole printing process does not require an extra protective atmosphere environment. Next, after 3D printing of complex models, the resulting models need to be cleaned with anhydrous ethanol to remove the effects of residual ink on accuracy. Eventually, the model was placed in a drying oven at 60 °C for 30 minutes to obtain the final specimen.

4.4 Fabrication of a tactile sensing system for e-skin *via* 3D printing

The designed circuit and electrode are accurately reproduced on flexible PET films through screen-printing technology. The circuit and electrode are made of conductive carbon paste, which needs to be mixed with diluent 783 in a certain proportion before use. Thereafter, the printed circuit and electrode were stored at 50 °C for about 1 h for drying. Next, the LFCIg ink is polymerized *in situ* on a flexible electrode by using a 3D printer ensures that the array as the sensing unit is appropriately prepared. Finally, the flexible circuit, sensor array and Jumper Wire interface were assembled to obtain the e-skin.

4.5 Measurements and characterization

The mechanical properties, including single tensile and cyclic tensile, as well as the self-healing properties of LFCIg were assessed using a universal material testing machine (AG-X plus, SHIMADZU) operating at a speed of 100 mm min^{-1}. The electromechanical stability tests were conducted using Flexible Electronic Test Devices by Shanghai Mifang electronic technology Co., Ltd. To minimize the impact of potential errors on the outcomes, the experiments were conducted in triplicate. The Differential Scanning Calorimetry (DSC) was tested by DSC-Q20. The ionogel that was fabricated underwent structural characterization using Fourier transform infrared (FT-IR) spectroscopy, which involved analyzing the wavenumber range of 500 to 4000 cm^{-1}. The conductivity of the ionogel was determined through an electrochemical workstation (CHI660D). To calculate the ionic conductivity, the formula $\sigma = R/(L \times A)$ was utilized, wherein L denotes the thickness of the LFCIg sample, R was the bulk resistance obtained from the Nyquist plot when $-Z'' = 0$, and A represents the effective overlap area between the sample and the electrode. The sensor resistance changes were collected in real time by using a digital multimeter (Keithley, 2450). The sensitivity of the sensor was determined using the gauge factor (GF) formula, which was calculated as $GF = (\Delta R/R_0)/\varepsilon$. Here, R_0 represented the initial resistance value, ΔR was the difference between the real-time measured resistance R and R_0, and ε was the stretch parameter. Similarly, the sensitivity of the pressure capacitance sensor and the ion skin comprising LFCIg was defined as $\delta = (\Delta C/C_0)/P$, where C_0 represented the original capacitance value and ΔC represented the change in capacitance corresponding to the pressure change P.

Conflicts of interest

There are no conflicts to declare.

Acknowledgements

This research was funded by the National Natural Science Foundation of China (22171266 and 11972005). This work

was also supported by the Fujian College Association Instrumental Analysis Center of Fuzhou University.

References

1 G. Balakrishnan, J. Song, C. Mou and C. J. Bettinger, *Adv. Mater.*, 2022, **34**, 2106787.
2 G. Li, K. Huang, J. Deng, M. Guo, M. Cai, Y. Zhang and C. F. Guo, *Adv. Mater.*, 2022, **34**, 2200261.
3 T. Li, Y. Wang, S. Li, X. Liu and J. Sun, *Adv. Mater.*, 2020, **32**, 2002706.
4 Z. Chen, D. Zhao, B. Liu, G. Nian, X. Li, J. Yin, S. Qu and W. Yang, *Adv. Funct. Mater.*, 2019, 29.
5 H. Niu, H. Li, S. Gao, Y. Li, X. Wei, Y. Chen, W. Yue, W. Zhou and G. Shen, *Adv. Mater.*, 2022, **34**, 2202622.
6 H. Qiao, S. Sun and P. Wu, *Adv. Mater.*, 2023, 2300593.
7 J. Qin, L. J. Yin, Y. N. Hao, S. L. Zhong, D. L. Zhang, K. Bi, Y. X. Zhang, Y. Zhao and Z. M. Dang, *Adv. Mater.*, 2021, **33**, 2008267.
8 Y. Ren, Z. Liu, G. Jin, M. Yang, Y. Shao, W. Li, Y. Wu, L. Liu and F. Yan, *Adv. Mater.*, 2021, **33**, 2008486.
9 J. Huang, S. Han, J. Zhu, Q. Wu, H. Chen, A. Chen, J. Zhang, B. Huang, X. Yang and L. Guan, *Adv. Funct. Mater.*, 2022, **32**, 2205708.
10 J. Huang, S. Peng, J. Gu, G. Chen, J. Gao, J. Zhang, L. Hou, X. Yang, X. Jiang and L. Guan, *Mater. Horiz.*, 2020, **7**, 2085–2096.
11 E. Sachyani Keneth, A. Kamyshny, M. Totaro, L. Beccai and S. Magdassi, *Adv. Mater.*, 2021, **33**, 2003387.
12 Q. Wu, S. Han, J. Zhu, A. Chen, J. Zhang, Z. Yan, J. Liu, J. Huang, X. Yang and L. Guan, *Chem. Eng. J.*, 2023, 454.
13 H. Xiang, X. Li, B. Wu, S. Sun and P. Wu, *Adv. Mater.*, 2023, **35**, 2209581.
14 B. Zhang, H. Li, J. Cheng, H. Ye, A. H. Sakhaei, C. Yuan, P. Rao, Y. F. Zhang, Z. Chen, R. Wang, X. He, J. Liu, R. Xiao, S. Qu and Q. Ge, *Adv. Mater.*, 2021, **33**, 2101298.
15 J. Chen, Y. Gao, L. Shi, W. Yu, Z. Sun, Y. Zhou, S. Liu, H. Mao, D. Zhang, T. Lu, Q. Chen, D. Yu and S. Ding, *Nat. Commun.*, 2022, **13**, 4868.
16 J. P. Gong, Y. Katsuyama, T. Kurokawa and Y. Osada, *Adv. Mater.*, 2003, **15**, 1155–1158.
17 Q. Liang, X. Xia, X. Sun, D. Yu, X. Huang, G. Han, S. M. Mugo, W. Chen and Q. Zhang, *Adv. Sci.*, 2022, **9**, 2201059.
18 Q. He, Y. Huang and S. Wang, *Adv. Funct. Mater.*, 2018, **28**, 1705069.
19 H. Lu, B. Wu, X. Le, W. Lu, Q. Yang, Q. Liu, J. Zhang and T. Chen, *Adv. Funct. Mater.*, 2022, **32**, 2206912.
20 S. Cheng, Z. Lou, L. Zhang, H. Guo, Z. Wang, C. Guo, K. Fukuda, S. Ma, G. Wang, T. Someya, H. M. Cheng and X. Xu, *Adv. Mater.*, 2022, **35**, 2206793.
21 B. Yiming, Y. Han, Z. Han, X. Zhang, Y. Li, W. Lian, M. Zhang, J. Yin, T. Sun, Z. Wu, T. Li, J. Fu, Z. Jia and S. Qu, *Adv. Mater.*, 2021, **33**, 2006111.
22 J. R. Sempionatto, J. A. Lasalde-Ramirez, K. Mahato, J. Wang and W. Gao, *Nat. Rev. Chem.*, 2022, **6**, 899–915.
23 C. Lu, C. Wang, J. Wang, Q. Yong and F. Chu, *Chem. Eng. J.*, 2021, **425**, 130652.
24 L. Cai, G. Chen, B. Su and M. He, *Chem. Eng. J.*, 2021, **426**, 130545.
25 X. Qu, W. Niu, R. Wang, Z. Li, Y. Guo, X. Liu and J. Sun, *Mater. Horiz.*, 2020, **7**, 2994–3004.
26 P. Yao, Q. Bao, Y. Yao, M. Xiao, Z. Xu, J. Yang and W. Liu, *Adv. Mater.*, 2023, 2300114.
27 X. Chang, M. Fan, C. F. Gu, W. H. He, Q. Meng, L. J. Wan and Y. G. Guo, *Angew. Chem., Int. Ed.*, 2022, 202202558.
28 E. L. Smith, A. P. Abbott and K. S. Ryder, *Chem. Rev.*, 2014, **114**, 11060–11082.
29 K. Zhao, K. Zhang, R. A. Li, P. Sang, H. Hu and M. He, *J. Mater. Chem. A*, 2021, **9**, 23714–23721.
30 S. Wang, L. Zhang, R. Ma, J. Yu, X. Zhang, C. Shi, L. Ma, T. Li, Y. Huang, Y. Hu, Y. Fan and Z. Wang, *Chem. Eng. J.*, 2023, **454**, 140022.
31 X. Sun, Y. Zhu, J. Zhu, K. Le, P. Servati and F. Jiang, *Adv. Funct. Mater.*, 2022, **32**, 2202533.
32 S. Duan, Q. Shi, J. Hong, D. Zhu, Y. Lin, Y. Li, W. Lei, C. Lee and J. Wu, *ACS Nano*, 2023, **17**, 1355–1371.
33 S. C. B. Mannsfeld, B. C. K. Tee, R. M. Stoltenberg, C. V. H. H. Chen, S. Barman, B. V. O. Muir, A. N. Sokolov, C. Reese and Z. Bao, *Nat. Mater.*, 2010, **9**, 859–864.
34 M. Cai, Z. Jiao, S. Nie, C. Wang, J. Zou and J. Song, *Sci. Adv.*, 2021, **7**, 8313.
35 X. Qu, Z. Liu, P. Tan, C. Wang, Y. Liu, H. Feng, D. Luo, Z. Li and Z. L. Wang, *Sci. Adv.*, 2022, **8**, 2521.
36 E. Davoodi, H. Montazerian, R. Haghniaz, A. Rashidi, S. Ahadian, A. Sheikhi, J. Chen, A. Khademhosseini, A. S. Milani, M. Hoorfar and E. Toyserkani, *ACS Nano*, 2020, **14**, 1520–1532.
37 H. Yuk, B. Lu, S. Lin, K. Qu, J. Xu, J. Luo and X. Zhao, *Nat. Commun.*, 2020, **11**, 1604.
38 D. P. A. Heiden, L. Lehner, M. Baumgartner, M. Drack, E. Woritzka, D. Schiller, R. Gerstmayr, F. Hartmann and M. Kaltenbrunner, *Sci. Robot.*, 2022, **7**, 2119.
39 H. Liu, C. Du, L. Liao, H. Zhang, H. Zhou, W. Zhou, T. Ren, Z. Sun, Y. Lu, Z. Nie, F. Xu, J. Zhu and W. Huang, *Nat. Commun.*, 2022, **13**, 3420.
40 M. A. Saccone, R. A. Gallivan, K. Narita, D. W. Yee and J. R. Greer, *Nature*, 2022, **612**, 685–690.
41 Z. Wang, H. Cui, M. Liu, S. L. Grage, M. Hoffmann, E. Sedghamiz, W. Wenzel and P. A. Levkin, *Adv. Mater.*, 2021, **34**, 2107791.
42 R. A. Li, K. Zhang, G. Chen, B. Su and M. He, *Chem. Mater.*, 2021, **33**, 5189–5196.
43 Z. Zhang, J. Luo, S. Zhao, S. Ge, J.-M. Y. Carrillo, J. K. Keum, C. Do, S. Cheng, Y. Wang, A. P. Sokolov and P.-F. Cao, *Matter*, 2022, **5**, 237–252.
44 R. A. Li, T. Fan, G. Chen, K. Zhang, B. Su, J. Tian and M. He, *Chem. Mater.*, 2020, **32**, 874–881.
45 M. Wu, J. Chen, Y. Ma, B. Yan, M. Pan, Q. Peng, W. Wang, L. Han, J. Liu and H. Zeng, *J. Mater. Chem. A*, 2020, **8**, 24718–24733.

46 Z. Chen, Y. Zhang, B. Zhu, Y. Wu, X. Du, L. Lin and D. Wu, *ACS Appl. Mater. Interfaces*, 2022, **14**, 19672–19682.
47 X. Ming, C. Zhang, J. Cai, H. Zhu, Q. Zhang and S. Zhu, *ACS Appl. Mater. Interfaces*, 2021, **13**, 31102–31110.
48 P. Shi, Y. Wang, W. W. Tjiu, C. Zhang and T. Liu, *ACS Appl. Mater. Interfaces*, 2021, **13**, 49358–49368.
49 J. H. Kim, K. G. Cho, D. H. Cho, K. Hong and K. H. Lee, *Adv. Funct. Mater.*, 2021, **31**, 2010199.
50 L. Shi, T. Zhu, G. Gao, X. Zhang, W. Wei, W. Liu and S. Ding, *Nat. Commun.*, 2018, **9**, 2630.
51 M. Wang, Z. Lai, X. Jin, T. Sun, H. Liu and H. Qi, *Adv. Funct. Mater.*, 2021, **31**, 2101957.
52 C. Dang, F. Peng, H. Liu, X. Feng, Y. Liu, S. Hu and H. Qi, *J. Mater. Chem. A*, 2021, **9**, 13115–13124.
53 W. Zhang, B. Wu, S. Sun and P. Wu, *Nat. Commun.*, 2021, **12**, 4082.
54 X. Yao, S. Zhang, L. Qian, N. Wei, V. Nica, S. Coseri and F. Han, *Adv. Funct. Mater.*, 2022, 2204565.
55 Z. Wang, Y. c Lai, Y. t Chiang, J. M. Scheiger, S. Li, Z. Dong, Q. Cai, S. Liu, S. h Hsu, C. c Chou and P. A. Levkin, *ACS Appl. Mater. Interfaces*, 2022, **14**, 50152–50162.
56 Q. Cui, X. Huang, X. Dong, H. Zhao, X. Liu and X. Zhang, *Chem. Mater.*, 2022, **34**, 10778–10788.
57 X. Su, X. Wu, S. Chen, A. M. Nedumaran, M. Stephen, K. Hou, B. Czarny and W. L. Leong, *Adv. Mater.*, 2022, 2200682.
58 L. Xu, Z. Huang, Z. Deng, Z. Du, T. L. Sun, Z. H. Guo and K. Yue, *Adv. Mater.*, 2021, **33**, 2105306.
59 J. Lu, J. Gu, O. Hu, Y. Fu, D. Ye, X. Zhang, Y. Zheng, L. Hou, H. Liu and X. Jiang, *J. Mater. Chem. A*, 2021, **9**, 18406–18420.
60 B. Yiming, X. Guo, N. Ali, N. Zhang, X. Zhang, Z. Han, Y. Lu, Z. Wu, X. Fan, Z. Jia and S. Qu, *Adv. Funct. Mater.*, 2021, **31**, 2102773.
61 S. Xiang, X. He, F. Zheng and Q. Lu, *Chem. Eng. J.*, 2022, **439**, 135644.
62 P. Zhang, I. M. Lei, G. Chen, J. Lin, X. Chen, J. Zhang, C. Cai, X. Liang and J. Liu, *Nat. Commun.*, 2022, **13**, 4775.